Development of Theranostics Albumin Auristatin Conjugates for Combining Chemotherapy with Boron Neutron Capture Therapy

Meiling Wang[2], Ivan A. Moskalev[2], Olga D. Zakharova[1], Anna I. Kasatova[3], Vladimir N. Silnikov[1], Tatyana V. Popova[1,2*], Tatyana S. Godovikova[1,2*]

[1]Department of Pharmacology, Institute of Chemical Biology and Fundamental Medicine, SB RAS, 630090 Novosibirsk, Russia

[2]Department of Natural Sciences, Novosibirsk State University, 630090 Novosibirsk, Russia

[3]Department of Nuclear Medicine, Budker Institute of Nuclear Physics, SB RAS, 630090 Novosibirsk, Russia

Corresponding Author*

Tatyana V. Popova,

Department of Pharmacology,

Institute of Chemical Biology and Fundamental Medicine,

Novosibirsk, Russia

E-mail: io197724@gmail.com

Tatyana S. Godovikova,

Department of Pharmacology,

Institute of Chemical Biology and Fundamental Medicine,

Novosibirsk, Russia

E-mail: t_godovikova@mail.ru

Received: 25-Jan-2024, Manuscript No. JBTW-24-125938; **Editor assigned:** 29-Jan-2024, PreQC No. JBTW-24-125938 (PQ); **Reviewed:** 12-Feb-2024, QC No. JBTW-24-125938; **Revised:** 19-Feb-2024, Manuscript No. JBTW-24-125938 (R); **Published:** 26-Feb-2024, DOI: 10.35248/2322-3308-13.1.007.

Abstract

Combining boron neutron capture therapy with chemotherapy can provide good therapy efficacy and is of great relevance today. In this study, we focused on serum albumin, a well-known drug delivery system, and developed homocysteine-functionalized boron albumin conjugate with chemotherapeutic molecules (monomethyl auristatin E, MMAE and auristatin F, MMAF). The new N-acylated homocysteine thiolactone bearing a cobalt bis (dicarbollide) derivative was used to create the fluorophore-albumin based construct. We report on the synthesis of a fluorophore-labeled boron-homocystamide conjugates of human serum albumin and their use in thiol-'click' chemistry to prepare a novel multifunctional constructs with the antitubulin agents MMAE or MMAF. We demonstrate that boron-equipped albumin conjugate with MMAE was more potent than MMAF conjugate, in the killing tumor cells. The half-maximal Inhibitory Concentration (IC_{50}) of the designed theranostics was not less than 0.034 μM relative to T98G glioma cells with the correlation coefficient not less than R=0.88, and not less than 0.97 μM relative U 87 glioma cells with the correlation coefficient not less than R=0.71. Both theranostics are observed *in vitro* in the cytoplasm of human glioblastoma cells T98G as dotted small vesicles indicating an endocytic mechanism of internalization.

Keywords: Boronated albumin theranostic conjugates • Monomethyl auristatins • Boron neutron capture therapy • Boron delivery agents

Introduction

Monomethyl auristatins E and F are potent derivatives of the natural product dolostatin 10 that inhibit tubulin polymerization in dividing cells and thereby induce apoptosis [1,2]. Since the original discovery of dolastatin 10 in 1987, the auristatins have attracted considerable interest due to their exceptional cytotoxicity, which is roughly 100-1000 times higher than that of doxorubicin, a previously often employed anticancer therapeutic [3]. Additionally, auristatins function as the vascular disrupting agents and damage the established tumor vessels. While this potential was intriguing to the scientific community, the high toxicity imposed severe constraints, which limited the practical applicability of auristatins for decades.

It was eventually discovered that auristatins are of great value as payloads in Antibody Drug Conjugates (ADCs), which led to the FDA-approved ADC brentuximab vedotin (Seattle Genetics) [2]. Seattle genetics has pioneered the selective delivery of auristatins to tumor cells by further modifying them to suitable analogues, including di-desmethylauristatin E and monomethylauristatin E, and conjugating them to tumor-targeting antibodies in the Fc region through a linker.

Currently, over 30 ADCs in clinical trials employ auristatins as payloads, and there is a great interest in the research community, both on academic and industrial sides, to further study these analogues [4]. However, in practice, the auristatin ADCs do display a number of side effects such as neutropenia, neuropathy, thrombocytopenia, and ocular toxicity [5]. A consequence of the adverse effects may be the reason why these ADCs are, for the most part, not currently considered as the primary cancer treatment options. Moreover, the subclonal diversity of the tumor cells in a single patient regarding their genetic, epigenetic, and phenotypic properties, known as intratumor heterogeneity, fundamentally restricts active tumor targeting to a limited population of tumor cells expressing the target molecule. In addition, their complex synthetic chemistry hindering industrial-scale manufacturing is a formidable challenge for clinical translation.

We are interested in this class of molecules as they could also feed our ongoing program in the development of prodrugs of the human serum albumin [6,7]. Human Serum Albumin (HSA) has been well established as a platform for various diagnostic and therapeutic applications [8,9]. HSA has been successfully used clinically as a noncovalent carrier for insulin (e.g., Levemir), GLP-1 (e.g., Liraglutine), and paclitaxel (e.g., Abraxane). As an excellent drug delivery carrier, albumin has been widely applied in the development of anticancer drugs [10]. It was discovered that auristatins are of great value as payloads in albumin drug conjugates [11-17]. It was demonstrated that auristatin-HSA conjugates exert potent activities on cancer cell. Until now, the latest research progress of albumin drug conjugates was that of Xinquan et al., [11]. They tried to replace the antibody of ADC (Antibody Drug Conjugate): Adcetris (CD30-VC-MMAE, VC-MMAE is the most successful linker payload in ADC) with albumin. The obtained conjugate HSA-VC-MMAE was broad-spectrum compared to Adcetris and could avoid the need for high antigen expression. However, to achieve similar *in vivo* potency, Adcetris (MMAE: 0.018 mg/kg) was significantly greater than conjugate HSA-VC-MMAE (Conjugate: 47 mg/kg, MMAE: 0.5 mg/kg). In summary, although albumin as a broad-spectrum drug carrier could obviously reduce the times of administration, its weak efficacy still limits its use.

Current anticancer research shows that a combination of multiple treatment methods can greatly improve the killing of tumor cells. It is speculated that combining chemotherapy with Boron Neutron Capture Therapy (BNCT) can provide good therapy efficacy and is of great relevance today [18,19]. BNCT, in which drugs containing enriched boron are

accumulated in tumor cells followed by their neutron beam radiation offers an advantage over conventional chemo and radiotherapies as it selectively targets tumor cells. Currently, some research groups developed maleimide-functionalized closo-dodecaborate and aimed to conjugate it to albumin [20-24]. Conjugation of albumin with undecahydro-closo-dodecaborate did not significantly affect cell viability in the absence of irradiation, as compared with the unmodified protein. However, neutron capture by this boron-containing albumin decreased the tumor cell survival. It was found that dodecaborated albumin conjugates induces an efficient boron neutron capture reaction because the albumin contained in conjugate is retained in the tumor and has a considerable potential to become an effective delivery system for BNCT in treating high-grade gliomas [25].

In this study, we reported on the synthesis of a fluorophore-labeled boron-homocystamide conjugates of albumin and their use in thiol-'click' chemistry to prepare a novel multifunctional constructs with the antitubulin agents (MMAE and MMAF) for combining chemotherapy with BNCT. We studied the tumor cell killing properties of the theranostics albumin auristatin conjugates in human glioma cells compared with boron-albumin conjugate and free MMAE or MMAF.

Materials and Methods

Chemicals, reagents, and facilities

The human glioblastoma T98G and U87 cell lines were received from the Russian cell culture collection (Russian Branch of the ETCS, St. Petersburg, Russia).

Unless otherwise indicated, all of the starting materials and solvents were obtained from commercial suppliers at the highest grade available and used without further purification. All reactions were monitored by Thin Layer Chromatography (TLC) on DC-Alufolien Kieselgel 60 F254 plates (Merck, Germany) with fluorescence F-254 and visualized with UV light. Column chromatography was carried out on silica gel (Acros Organics, 0,060-0,200 mm).

Drug-linker conjugates (mc-vc-pab-MMAE and mc-vc-pab-MMAF) were provided by Pharmaceutical company Suzhou Jianhua Co., Ltd. (Suzhou, China). D,L-Homocysteine Thiolactone Hydrochloride (DL-HTL × HCl) Hydrochloride and the Human Serum Albumin (HSA) was obtained from Sigma-Aldrich Chem. Co. (St. Louis, MO, USA). The product number of HSA used was A3782.

The concentrations of albumin solutions were determined by absorption at 278 nm, pH 7.4, using the molar extinction coefficient $\varepsilon = 3.7 \times 10^4\ M^{-1}cm^{-1}$ [26].

Electronic absorption spectra were acquired on a UV-1800 spectrometer (Shimadzu, Japan).

IR spectra were recorded in the range 4000-400 cm^{-1} using a Genesys 64 v/vis spectrometer.

^1H NMR, ^{13}C NMR and ^{19}F NMR spectra were recorded on AV-300, AV-400, AV-600 NMR spectrometer (Bruker, Germany). The spectra were detected at 25°C in 5 mm NMR sample tubes. D_2O (δ 3.8 ppm), acetone-d6 (δ 2.05 ppm) was used as an external reference for chemical shifts in ^1H NMR spectra. Acetone-d6 (δ 206.35 ppm) was used as an external reference for chemical shifts in ^{13}C NMR spectra. Chemical shifts (δ) are reported in parts per million (ppm).

ESI mass spectra were registered on Agilent ESI MSD XCT Ion Trap (Agilent Technologies, Santa Clara, CA, USA) in positive or negative mode at The Joint Center for genomic, proteomic and metabolomics studies (ICBFM SB RAS, Russia).

Mass spectra of proteins were recorded on Bruker Autoflex Speed (Bruker Daltonics, Germany) MALDI-ToF mass spectrometer in a positive linear mode. A smartbeam-II laser was used. 2,5-Dihydroxyacetophenone (2,5-DHAP) was used as a matrix. Protein samples were desalted by ZipTip C4 pipette tips. A 2 µL of the protein sample solution was mixed with 2 µL of a 2% TFA (Trifluoroacetic Acid). To the latter solution 2 µL of the matrix (2,5-DHAP) was added. The mixture was pipetted up and down until the crystallization starts. Mass spectra were obtained by averaging 3,000 laser shots. External calibration was provided by $[M+H]^+$ HSA at m/*z* 66.5 kDa.

SDS-PAGE. Human serum albumin conjugates were analyzed by sodium dodecyl sulfate polyacrylamide gel electrophoresis using 7% PAAG under Laemmli condition without the addition of DTT or DTT with subsequent Coomassie Brilliant Blue (BioRad) staining.

Low molecular weight materials (MW <3 kDa) were removed from solutions of polymer conjugates by centrifugal filtration using Centricon concentrators with a MWCO of 3 kDa (Amicon Centriprep YM30, Millipore, Bedford, MA).

Synthesis of the homocysteine thiolactone containing bis(dicarbollide) complex of cobalt (III)

The synthetic route for the homocysteine thiolactone containing bis(dicarbollide) complex of cobalt (III) is shown in Figure 1. The original mass spectrometry and NMR spectral details of the synthesized compounds are provided in Figures S1 and S2.

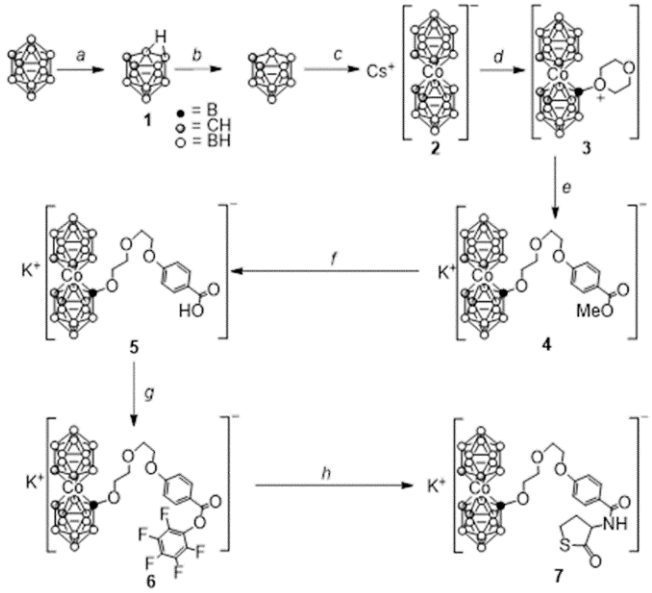

Figure 1. General synthetic route for the homocysteine thiolactone containing bis(dicarbollide) complex of cobalt (III). Reagents and conditions: (a) — 1) 5% alcohol solution sodium hydroxide, boiling, 12 h, 2) 1 M HCl, 3) H_2O, Me_3NHCl; (b) — 40% aqueous sodium hydroxide; (c) — 1) $CoSO_4 \times 7\ H_2O$ (1.2 excess), 30 min, 2) water solution of CsCl; (d) — $BF_3 \times Et_2O$ (8.3 excess) in dioxane, boiling, 5 h; (e) — 3×10^{-4} M K_2CO_3 in acetone, methyl ether of p-hydroxybenzoic acid (2.9 excess), 60°C, 1 h; (f) — 1 M KOH, 1 day; (g) — pentafluorophenol (1.08 excess), DCC (1.04 excess) in ethyl acetate, 4 h at room temperature; (h) — DL-HTL × HCl (1.1 excess), DIPEA (1.46 excess) in DMF, 60°C, 4 h.

Note: (●) B; (◍) CH; (○) BH.

Compound 2 was synthesized using previously reported experimental protocols [27]. One of the convenient methods for the functionalization of the bis(dicarbollide) complex of cobalt (III) is the preparation of its oxonium derivative (3) entering into a nucleophilic substitution reaction. The resulting nucleophilic attack product (4) contains a linker for further modification. Compound 3 was synthesized according to the adapted procedure [28]. The interaction of compound 3 with p-hydroxybenzoic acid methyl ester leads to the formation of compound 6 according to the procedure [29]. Then, the compound 4 was subjected to basic hydrolysis to give the compound (5), which was further activated with pentafluorophenol in the presence of dicyclohexylcarbodiimide to produce compound 6 at 77% yield. Detailed synthetic procedures and spectroscopic data of synthesized compound are given in Supporting Information.

Synthesis of N-substituted boron-homocysteine thiolactone K[3,3'-Co($B_9C_2H_{11}$)(8-$B_9C_2H_{11}OCH_2CH_2OCH_2CH_2OC_6H_4CONH$-$C_4H_5SO$)] (compound 7, Figure 1)

A solution of DL-HTL × HCl in DMF (0.1 mL, 0.065 mmol) was mixed with 0.015 mL of DIPEA and added to a DMF solution of the compound 6 (0.2 mL, 0,059 mmol). The resulting mixture was heated to 60°C for 4 hours with a reverse refrigerator. After that, solvent was evaporated on a rotary

evaporator and 0.35 mL of ethyl acetate was added. The organic phase was washed with water solution of citric acid (10%, 2 × 0.11 mL) and then by water solution of potassium carbonate (10%, 2 × 0.12 mL). The organic phase was dried with dehydrated sodium sulfate and the solvent was evaporated on a rotary evaporator. The resulting compound was purified by column chromatography on silica gel (Eluent: CH_2Cl_2/acetone 10:16 by volume) giving 0.026 g of an orange oil.

The yield of the product 7 65%. IR (KBr, cm^{-1}): 3400 ν(N-H); 2990, 2910, 2840 ν(C-H); 2550 ν(B-H); 1650 ν(C=O); 1620 δ(N-H); 1500, 1450 ν(C-N); 1230, 1120, 1090 ν(O-C-O)asym. UV-vis (CH2Cl2): λ_{max} 246 nm (ε= (2.63 ± 0.02) × 105), λ_{max} 448 nm (ε= (4.10 ± 0.01) × 102). 1H NMR (Acetone-d6, δ, ppm): 7.88 (2H, d, H-9); 7.02 (2H, d, H-8); 4.94 (1H, m, H-12); 4.28 (4H, s, H-1, H-2); 4.19 3.83 3.58 2.87 (8H, t, H-6, H-5, H-4, H-3); 3.49 (1H, m, H-14α); 3.35 (1H, m, H-14β); 2.66 (1H, m, H-13α), 2.34 (1H, m, H-13β). 13C NMR (Acetone-d6, δ, ppm): 205.4 (1C, s, C-15); 167.3 (1C, s, C-11); 162.8 (1C, s, C-7); 130.0 (1C, s, C-9); 127.2 (1C, s, C-10); 115.1 (1C, s, C-8); 72.9 (1C, s, C-6); 70.0 (1C, s, C-5); 69.3 (1C, s, C-3); 68.6 (1C, s, C-4); 59.7(1C, s, C-12); 55.2 (1C, s, C-2); 47.3 (1C, s, C-1); 31.4 (1C, s, C-14); 27.5 (1C, s, C-13). Mass spectrometry (ESI, negative) m/z: calculated for 647.1; measured value MW 646.8.

Synthesis and characterization of multifunctional human serum albumin-therapeutic conjugates

HSA-Cy5: The synthesis of HSA-Cy5 was adapted from Chubarov et al., [30].

HSA Cy5 HcyCo($B_9C_2H_{11}$)$_2$: A solution of HSA-Cy5 in PBS buffer (2.235 mL, 8.4 × 10^{-4} M, 1.88 μmol) was mixed with Co($B_9C_2H_{11}$)$_2$-HTL (compound 7) dissolved in DMSO (118 μL and 12.2 μmol). Molar ratio Co($B_9C_2H_{11}$)$_2$-HTL/HSA was 6.5 and a volume ratio DMSO/PBS in the reaction mixture was 0.05. The reaction was carried out for 42 h at 37°C. Purification of the final conjugate was performed using centricons (Amicon Centriprep YM30, Millipore, Bedford, MA) that pass molecules with a molecular weight of less than 3,000 Da. For washing, 10% (by volume) DMSO in PBS, 10 volumes of the reaction mixture, and then PBS, 10 volumes of the reaction mixture were used. The yield of HSA-Cy5-HcyCo($B_9C_2H_{11}$)$_2$ was ~66%. UV-vis (PBS buffer, pH 7.4): λ_{max} 268 nm (ε= (10.45 ± 0.1) × 10^4), λ_{max} 313 nm (ε= (8.22 ± 0.2) × 10^4), λ_{max} 652 nm (ε= (6.64 ± 0.1) × 10^4). Mass spectrometry (MALDI-TOF) m/z: measured average MW for HSA-Cy5-HcyCo($B_9C_2H_{11}$)$_2$ is 67,982 Da corresponds to two residues of HcyCo($B_9C_2H_{11}$)$_2$ per one molecule of HSA (calculated MW for HcyCo($B_9C_2H_{11}$)$_2$ 647 Da). Inductively coupled plasma atomic emission spectroscopy: 1.99 ± 0.08 ppm of boron (total) was detected at a conjugate quantity in the analyzed sample 0.035 μmol. It corresponds to 2.01 ± 0.05 of the HcyCo($B_9C_2H_{11}$)$_2$ residues per albumin.

HSA Cy5 HcyCo($B_9C_2H_{11}$)$_2$-MMAF and HSA Cy5 HcyCo($B_9C_0H_{11}$)$_2$-MMAE: Purified HSA-Cy5-HcyCo($B_9C_2H_{11}$)$_2$ in PBS buffer (524 μL, 0.7 × 10^{-3} M, 0.37 μmol) was mixed with mc-vc-pub-MMAE or mc-vc-pub-MMAF dissolved in DMSO (52.4 μL and 2.8 μmol). The molar ratio peptide HSA-Cy5-HcyCo($B_9C_2H_{11}$)$_2$ was 7.5, and a volume ratio DMSO/PBS in the reaction mixture was 0.1. The reaction was carried out for 18 h at 37°C. Purification of the final conjugates was performed out in the same way as for HSA Cy5 HcyCo($B_9C_2H_{11}$)$_2$. The yield of HSA-Cy5-HcyCo($B_9C_2H_{11}$)$_2$-MMAE~86.77%. UV-vis (PBS buffer, pH 7.4): λ_{max} 255 nm (ε= (15.0 ± 0.1) × 104), λ_{max} 313 nm (ε= (8.22 ± 0.2) × 10^4), λ_{max} 654 nm (ε= (6.64 ± 0.1) × 10^4). Mass spectrometry (MALDI-TOF) m/z: Measured average MW for HSA-Cy5-HcyCo($B_9C_2H_{11}$)$_2$-MMAE is 70,615 Da corresponds to two residues of MMAE per one molecule of HSA (calculated MW for HcyCo($B_9C_2H_{11}$)$_2$ 647 Da, calculated MW for mc-vc-pub-MMAE 1,316 Da). The yield of HSA-Cy5-HcyCo($B_9C_2H_{11}$)$_2$-MMAF was ~84.8%. UV-vis (PBS buffer, pH 7.4): λ_{max} 255 nm (ε= (16.25 ± 0.1) × 104), λ_{max} 313 nm (ε= (8.22 ± 0.2) × 10^4) λ_{max} 654 nm (ε= (6.64 ± 0.1) × 10^4). Mass spectrometry (MALDI-TOF) m/z: Measured average MW for HSA-Cy5-HcyCo($B_9C_2H_{11}$)$_2$-MMAF is 70,643 Da corresponds to 2 residues of MMAF per one molecule of HSA (calculated MW for HcyCo($B_9C_2H_{11}$)$_2$ 647 Da, calculated MW for mc-vc-pub-MMAF 1330 Da).

Cell viability assay (MTT test)

The effect of the modified protein samples on human glioma cell lines (U87 and T98G) was performed using the MTT assay [31]. The cells were grown to exponential growth phase further seeded in 96-well plates. Cell concentration was 2000 cells per well. Before treatment, the cells were incubated for 72 h. After that they were treated with medium containing albumin and its conjugates (HSA, HSA Cy5 HcyCo($B_9C_2H_{11}$)$_2$, HSA Cy5 HcyCo($B_9C_2H_{11}$)$_2$-MMAF, HSA Cy5 HcyCo($B_9C_2H_{11}$)$_2$-MMAE, HSA+mc-vc-pub-MMAF, HSA+mc-vc-pub-MMAE). Conjugate concentrations ranged from 0.02 to 30 μM, equivalent to the protein content. The treatment was performed at 37°C for 72 h. After that, MTT was added to a concentration of 0.5 mg/mL. After incubation at 37°C for 2 h, the medium was removed, and each well was added by 100 μL of isopropanol to dissolve the formazan crystals. The plate was analyzed using a Multiscan FC microplate reader (Thermo Fisher Scientific Corporation) with an absorbance peak at 570 nm. The absorption intensity at 620 nm was used as a baseline. Three independent tests for each protein sample were performed. Data are presented as means with standard deviations.

Intracellular distribution of multifunctional human serum albumin-therapeutic conjugates *in vitro*

T98G human glioblastoma cells (10^5 cells/mL, 100 μL) in IMDM containing 10% FBS, penicillin and streptomycin were seeded into 96-well optical bottom plates with a coverslip base (Thermo Scientific™ Nunc™ MicroWell™). After preincubation for 17 h in a humidified atmosphere containing 5% CO_2, the medium was replaced with fresh medium containing HSA-Cy5-HcyCo($B_9C_2H_{11}$)$_2$-MMAE or HSA-Cy5-HcyCo($B_9C_2H_{11}$)$_2$-MMAF conjugate (20 μM). Time-lapse images were sampled every 5 min over a period of 1.5 h (microscope OLYMPUS IX83P2ZF, Japan). After that, the cells were incubated at 37°C for 3 h, washed 3 times with PBS. Further, the cells were fixed in 4% formaldehyde in PBS at room temperature for 20 min, washed two times with PBS and counterstained with DAPI (Fluoroshield™ with DAPI, Sigma-Aldrich). The intracellular localization of the HSA conjugates was evaluated using Cy5 red fluore scence (λ_{ex}=633 nm, λ_{em}=699 nm). The intracellular distribution of nuclei stained with DAPI was observed by fluorescence of DAPI (λ_{ex}=405 nm, λ_{em}=425-475 nm). Images were processed in ImageJ program.

Results and Discussion

As a promising approach to improve the tumor selectivity of anticancer drugs, the prodrug is a bioreversible medication that is specifically converted to the active drug by chemical or enzymatic transformation in the tumor microenvironment, which can considerably reduce the chemotherapy-induced side effects [32,33]. To harness the intrinsic transport properties of albumin yet improve the therapeutic index of current *in situ* albumin-binding prodrugs, authors [11] developed albumin-drug conjugates with a controlled loading that achieved better antitumor efficacy. Here, Model Drug Monomethyl Auristatin E (MMAE) was conjugated *ex vivo* to Cys34 of albumin *via* a cathepsin B-sensitive dipeptide linker to ensure that all drugs would be bound specifically to albumin. The utility of Cys34 in protein modification cannot be overstated. However, DTNB (5,5′-dithio-bis(2-nitrobenzoic acid)) titrations indicate the sulfhydryl titer for most commercial plasma HSA preparations is approximately 30%-40% [34,35]. In healthy subjects, Cys34 is mainly present in a reduced form (about 70%) (HSAred) while 25-30% is reversibly oxidized as a mixed disulfide, mainly with cysteine or in minor amounts with cysteinyl glycine, homocysteine and glutathione (HSAox) [35]. Very small amounts (3%-4%) of irreversibly oxidized forms, e.g., sulfinate and sulfonate, are also found [33]. Pathologic conditions, like kidney or liver diseases, may increase the level of oxidized HSA to 70% [36,37]. The heterogeneity of HSA is central to its physiological role and presents a complication for protein modification, but that is the biological reality. For the synthesis of albumin-drug conjugate with multiple payloads MMAE, a controlled reduction by TCEP was first used to expose more reactive thiols from disulfide bonds on albumin for conjugation [11]. However, partial reduction and subsequent addition of multiple drugs to albumin may affect the structure of albumin, which has been reflected in changes to the secondary structure of albumin-drug conjugate.

We previously reported using the reactivity of a thiolactone homocysteine (a cyclic thioester) as a latent thiol functionality in thiol-'click' chemistry for the synthesis of HSA-based theranostic agents [6,7,23,24,38]. The thiol was released by nucleophilic ring-opening (aminolysis) by amino groups on the HSA and subsequently reacted with a thiol 'scavenger' (a maleimide of the drug). Important aspect of our work

is that by achieving an optimal drug-to-albumin ratio through site-specific conjugation, we minimize the change in structure to albumin, which is important for achieving antitumor efficacy [6,7]. Similar to our work, other strategies on albumin-drug complexes have focused *ex vivo* covalent conjugation. For example, there was earlier literature that used the same MMAE payload and linker covalently conjugated to albumin [13,14]. In this work, albumin was thiolated to allow for ~4 MMAE molecules per albumin and allow for conjugation for RGD peptide for cell targeting. However, this conjugate failed to retain the intrinsic properties of albumin due to its non-specific conjugation through lysine.

Here, we use a thiolactone derivative as a functional handle for site-specific coupling of a bis(dicarbollide) complex of cobalt (III) and auristatins to HSA. The construction of boron-albumin auristatin conjugates is illustrated in Figure 2.

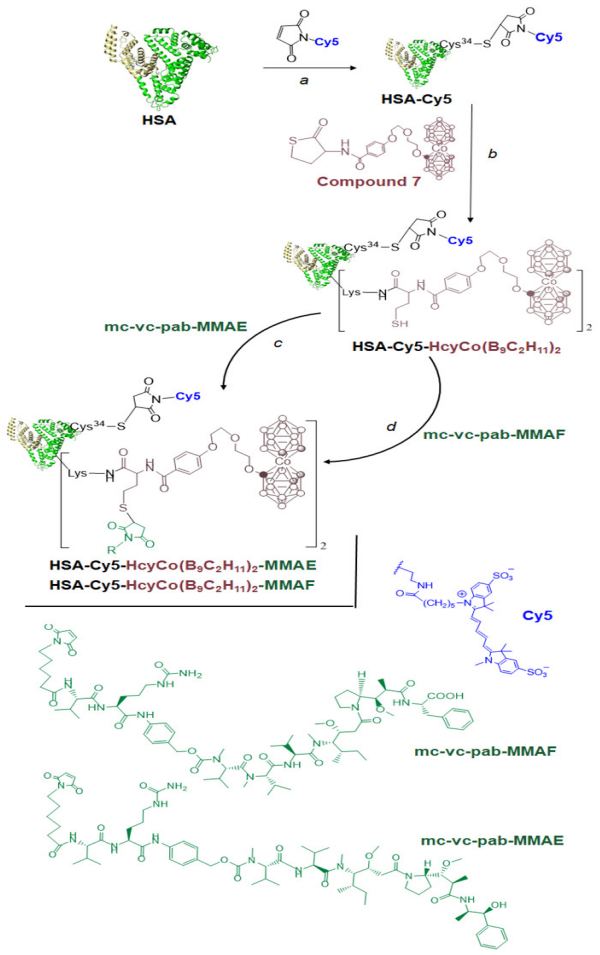

Figure 2. The constructing pathway of the new conjugates for BNCT: HSA-Cy5-HcyCo($B_9C_2H_{11}$)$_2$-MMAF and HSA-Cy5-HcyCo($B_9C_2H_{11}$)$_2$-MMAE.

HSA was preliminarily modified with the Cy5 dye at the cysteine residue 34 according to the method [30], to obtain the HSA-Cy5 conjugate (Figure 2, path a). The conjugation reaction of N-substituted boron-homocysteine thiolactone to HSA-Cy5 (Figure 2, path b) was performed in PBS buffer (pH 7.4) at 37°C. Low-molecular-weight homocysteine derivatives were removed from the HSA conjugates by centrifugal filtration with Centricon concentrators having a molecular weight cut-off of 3,000 Da. The resulting conjugate HSA-Cy5-HcyCo($B_9C_2H_{11}$)$_2$ UV-Vis spectrum contains a band at 650 nm, which matches the presence of Cy5 dye in this structure (Figure 3A). The successful synthesis of HSA-Cy5-HcyCo($B_9C_2H_{11}$)$_2$ was confirmed by inductively coupled plasma atomic emission spectroscopy: 2.0 HcyCo($B_9C_2H_{11}$)$_2$ residues per albumin on average.

The MALDI mass spectrometry data indicate mass increases of the HSA-Cy5-HcyCo($B_9C_2H_{11}$)$_2$ by 2633 and 2661 Da for HSA-Cy5-HcyCo($B_9C_2H_{11}$)$_2$-MMAE and HSA-Cy5-HcyCo($B_9C_2H_{11}$)$_2$-MMAF respectively (Figure 3B). This corresponds to the addition of 2 residues of each maleimide reagent per protein molecule.

Modification of HSA-Cy5-HcyCo($B_9C_2H_{11}$)$_2$ with maleimide auristatins (mc-vc-pab-MMAE and mc-vc-pab-MMAF) leads to a slight decrease in the mobility of the modified albumin conjugates in protein gel electrophoresis (Figure 3C), it can be explained by an increase in the mass of the conjugates (Figure 3B).

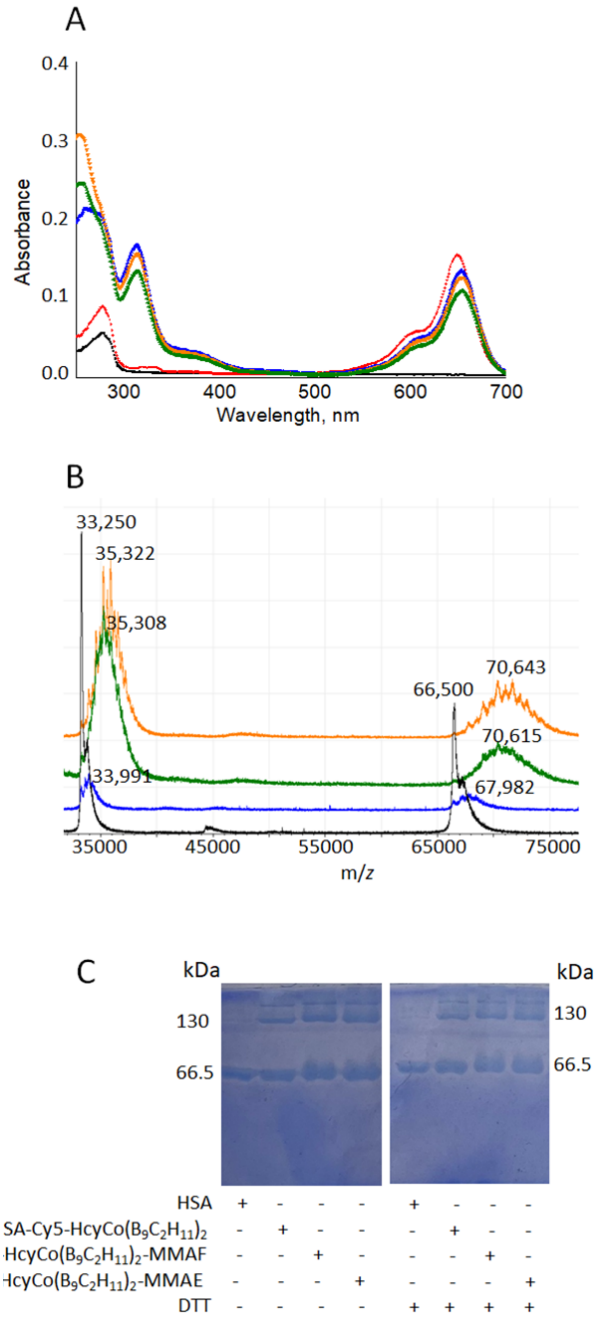

Figure 3. Characterizations of multifunctional human serum albumin conjugates. (A): UV-vis spectra of HSA and its homocystamides in PBS buffer, pH 7.4. HAS-black; HSA-Cy5-red; HSA-Cy5-HcyCo($B_9C_2H_{11}$)$_2$-blue, HSA-Cy5-HcyCo($B_9C_2H_{11}$)$_2$-MMAF-orange, HSA-Cy5-HcyCo($B_9C_2H_{11}$)$_2$-MMAE-green; (B): MALDI-TOF spectra of HAS-black; HSA-Cy5-HcyCo($B_9C_2H_{11}$)$_2$-blue, HSA-Cy5-HcyCo($B_9C_2H_{11}$)$_2$-MMAF-orange, HSA-Cy5-HcyCo($B_9C_2H_{11}$)$_2$-MMAE-green; (C): SDS-PAGE of homocystamide conjugates of the HSA under Laemmli conditions with subsequent Coomassie blue staining. **Note:** (——) HSA; (——) HSA -Cy5; (——) HSA-Cy5-HcyCo($B_9C_2H_{11}$)$_2$; (——) HSA-Cy5-HcyCo($B_9C_2H_{11}$)$_2$ -MMAF; (——) HSA-Cy5- HcyCo($B_9C_2H_{11}$)$_2$-MMAE.

In vitro experiments

MTT assays were utilized to evaluate the *in vitro* cellular proliferation inhibitions of HSA-Cy5-HcyCo($B_9C_2H_{11}$)$_2$-MMAE and HSA-Cy5-HcyCo($B_9C_2H_{11}$)$_2$-MMAF conjugates against human glioma cells. Glioma stem cells and other cells that exist in the glioma microenvironment play a crucial role in mediating glioma immune escape, tumor invasion, and recurrence [39]. The cysteine cathepsin family plays a prominent role in the immune escape of glioma [40-42]. A dipeptide (valine-citrulline) linker, cleavable by lysosomal proteases (e.g., cathepsin B), has been used us to link auristatins to boron-albumin. U87 and T98G cell lines were exposed to increasing albumin-based conjugates concentrations yielding dose-dependent proliferation inhibition after 72 hours of treatment (Figure 4). The cytotoxicity of the HSA-Cy5-HcyCo($B_9C_2H_{11}$)$_2$ conjugate, which was not modified with auristatin reagents, was insignificant in both cell lines.

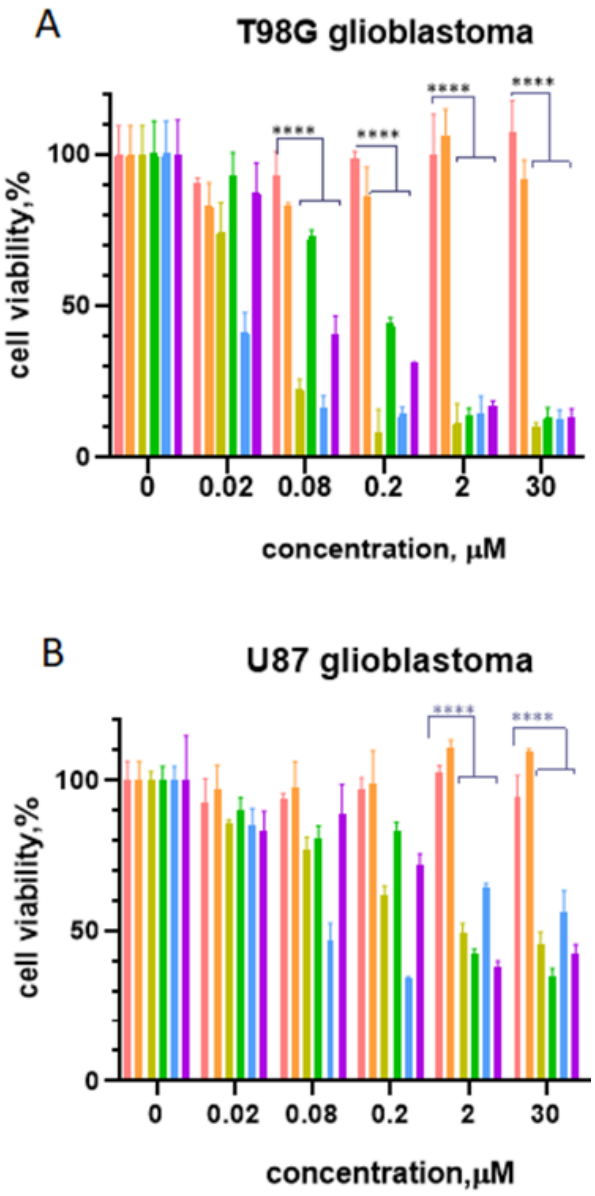

Figure 4. Cell viability of T98G and U87 cells treated with free auristatins in the presence of HSA and HSA Cy5-HcyCo($B_9C_2H_{11}$)$_2$, HSA Cy5-HcyCo($B_9C_2H_{11}$)$_2$-MMAE and HSA Cy5-HcyCo($B_9C_2H_{11}$)$_2$-MMAF conjugates for 24 h. (A): the cytotoxicity assays performed in T98G cell line; (B): the cytotoxicity assays performed in U87 cell line. The dose of auristatin and its equivalence was from 0.02 to 30 μM. All data are presented as mean ± SD (n=3). Two-way ANOVA was used for comparisons of more than two sets of data. **** –p-value ≤ 0.0001

Note: ( ) HSA; ( ) HSA-Cy5-HcyCo($B_9C_2H_{11}$)$_2$; ( )HSA-Cy5-HcyCo ($B_9C_2H_{11}$)$_2$-MMAE; ( )HSA-Cy5-HcyCo($B_9C_2H_{11}$)$_2$-MMAF; ( ) HSA+MMAE; ( ) HSA+MMAF.

Auristatin-HSA conjugates showed improved cellular growth inhibition in cathepsin B overexpressed U87 and T98G cells compared to boron-containing albumin, indicating auristatins could be released and inhibit the proliferation of glioma cancer cells, which encourages us for further *in vivo* investigation. Compared to the MMAF-albumin conjugate, the MMAE-albumin conjugate exhibited a 4-4.5-fold increase in potency when tested on T98G. Further, this conjugate was found to kill U87 cell type less effectively than T98G with IC_{50} values of 0.97 μM (Table 1). Furthermore, taking into account the IC_{50} values of free MMAE and free MMAF, we see that free MMAE is also more cytotoxic than the MMAF.

Table 1: The half-maximal Inhibitory Concentration (IC_{50}) for HSA homocystamides and controls (mixtures HSA+MMAF, HSA+MMAE).

Cells	Sample	IC_{50}	R
T98G	HSA-Cy5-HcyCo($B_9C_2H_{11}$)$_2$-MMAE	0.034	0.99
	HSA+MMAE	0.01	0.99
	HSA-Cy5-HcyCo($B_9C_2H_{11}$)2-MMAF	0.147	0.99
	HSA+MMAF	0.044	0.98
U87	HSA-Cy5-HcyCo($B_9C_2H_{11}$)$_2$-MMAE	0.97	0.89
	HSA+MMAE	0.173	0.71
	HSA-Cy5-HcyCo($B_9C_2H_{11}$)$_2$-MMAF	1.16	0.96
	HSA+MMAF	1.02	0.8

Confocal microscopy was used in order to confer the intracellular uptake and distribution of the theranostic borated albumin conjugates in T98G cells. The cells were incubated with HSA-Cy5-HcyCo($B_9C_2H_{11}$)$_2$-MMAE or HSA-Cy5-HcyCo($B_9C_2H_{11}$)$_2$-MMAF conjugate (20 μM) for 3 h. Since the far-red fluorescence of Cy5 does not overlap with cellular autofluorescence, the conjugates were monitored in cells by the fluorescence of Cy5 covalently attached to the conjugate (emission at 699 nm with excitation at 633 nm).

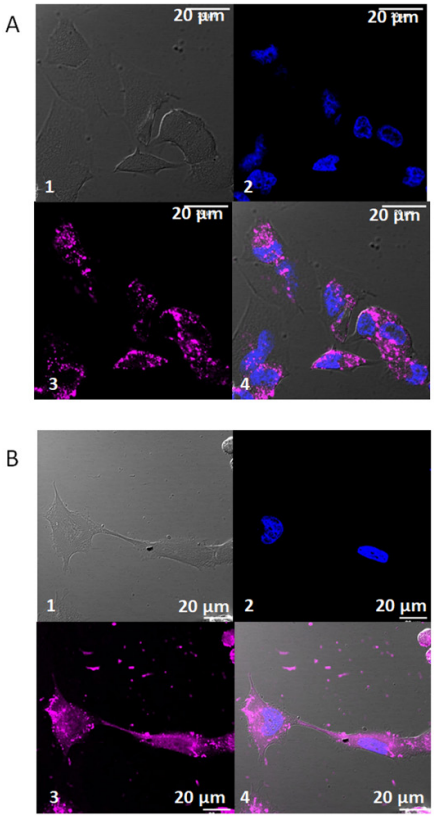

Figure 5. Representative images of confocal microscopy analysis of the T98G cells treated with the fluorescent HSA-Cy5-HcyCo($B_9C_2H_{11}$)$_2$-MMAE and HSA-Cy5-HcyCo($B_9C_2H_{11}$)$_2$-MMAF conjugates (20 μM) for 3 h. Cell nuclei were stained with DAPI. The conjugates are visible as a red color. Scale bars: 20 μm. (A): HSA-Cy5-HcyCo($B_9C_2H_{11}$)$_2$-MMAE; (B): HSA-Cy5-HcyCo($B_9C_2H_{11}$)$_2$-MMAF; 1-live cell image, 2-DAPI fluorescence, 3-conjugate's fluorescence, 4-merged 2 and 3.

Confocal microscopy images (Figure 5) showed the presence of the both conjugates as dotted small vesicles distributed in the cytoplasm of cells. Thus, it can be assumed that there is an endocytic mechanism of internalization [43]. Orthogonal projections of z-stack acquisitions showed that vesicles and endocytic structures were indeed present inside the treated cells (Figure 6). No critical differences in the uptake and distribution of the both conjugates were found.

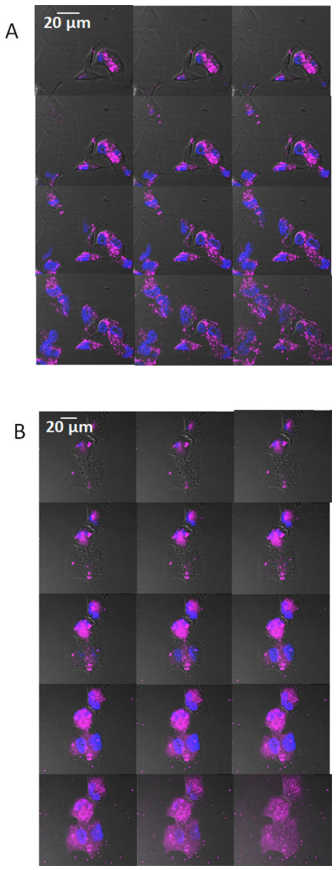

Figure 6. Gallery of merged images acquired along the z-axis of DAPI-stained T98G cells treated with the HSA conjugates. Cell nuclei are visible as a blue color. Conjugates are visible as a red color. Every subsequent image was taken 0.41 µm higher than the previous one. Scale bars: 20 µm. (A): HSA-Cy5-HcyCo($B_9C_2H_{11}$)$_2$-MMAE; (B): HSA-Cy5-HcyCo($B_9C_2H_{11}$)$_2$-MMAF.

Monomethylauristatin F is an auristatin that possesses a negatively charged C-terminal phenylalanine residue that limits cell permeability, in contrast to monomethylauristatin E, which is uncharged and freely cell permeable [44]. Intracellular linker proteolysis of monomethylauristatin E conjugates may, therefore, expose surrounding normal tissues to free drug that may induce toxicity. The risk of toxicity will be reduced when MMAF-albumin conjugate is used. It is also plausible that the accumulation of albumin-drug conjugate within the cells will by far compensate for the differences in intrinsic activity, especially when prolonged uptake can be ensured, for instance, by ensuring that the receptor-mediated uptake is taking place efficiently.

The delivery method of albumin to tumor tissues is passive because of the enhanced permeability and retention effect [45], but also active due to Secreted Protein Acidic and Rich in Cysteine (SPARC) and gp60 receptors [46]. These receptors are known to be highly expressed in high-grade glioma cells, and treatment with albumin-containing compounds using SPARC, which is a target of active transport [47,48]. Albumin can to target overexpressed gp-60 and SPARC receptors, allowing an enhanced drug uptake and bypassing drug efflux mechanisms. Moreover, it was found that increases in Caveolin-1 expression resulted in higher uptake of albumin [49]. Albumin enters through caveolae with the Fc-receptor, moves along actin, and reaches the early endosome, where some of them are sorted for lysosomal degradation, and others are directly transported outside the cells through exocytosis. The fact remains that as long as cancer cell biology is taken into account, albumin-binding proteins and caveolin-1–related roles seem to be tightly dependent on the cancer cell type. We believe that this may be responsible for the difference in IC_{50} values for auristatin-HSA conjugates in various cancer cell types. Further studies are required to clarify the specifics of this issue.

Conclusion

Albumin-driven delivery of therapeutics and imaging agents has become a popular technology, in parallel to antibody-driven targeting strategies. Recently, nano carrier-based boron delivery system, such as *closo*-dodecaborate-albumin conjugate, has been developed in order to achieve efficient BNCT. The conjugation of bimodal HSA with undecahydro-closo-dodecaborate little reduce human glioma cell line viability in the absence of irradiation but allowed for neutron capture and decreased tumor cell survival under epithermal neutron flux.

In this paper, we synthesized N-substituted boron-homocysteine thiolactone as a conjugation system for albumin functionalization by auristatins. The new N-acylated homocysteine thiolactone bearing a cobalt bis(dicarbollide) derivative was used to create the fluorophore-albumin based construct. Boron-homocysteine thiolactone was found to possess a high efficacy of conjugation to albumin. We report on the synthesis of a fluorophore-labeled boron-homocystamide conjugates of human serum albumin and their use in thiol-'click' chemistry to prepare a novel multifunctional constructs with the antitubulin agents MMAE or MMAF. We demonstrate that boron-equipped albumin conjugate with MMAE was more potent than MMAF conjugate, in the killing tumor cells.

The strategy of preparation of auristatin-modified boron-albumin conjugates proposed in this work could provide new ideas for the development of new generational albumin drug conjugates. Further studies are required to use them in a complete treatment of diseases.

Acknowledgments

We thank the Joint Center for genomic, proteomic and metabolomics studies (ICBFM SB RAS) for obtaining mass-spectra.

Author Contributions

Study conception and design: V.N.S. and T.S.G.; syntheses: M.W. and I.A.M.; data collection: M.W., I.A.M., O.D.Z. and A.I.K.; analysis and interpretation of results: T.V.P and T.S.G.; draft manuscript preparation: T.V.P and T.S.G; figures preparing: T.P.V. and O.D.Z. All authors reviewed the results and approved the final version of the manuscript.

Funding

This work was supported by the Russian state-funded project for ICBFM SB RAS (grant number 121031300042-1).

Data Availability

Original data is available from the authors upon request.

Declarations

Ethics approval and consent to participate: Not applicable.

Informed consent: Not applicable.

Consent for publication: Not applicable.

Research involving human participants or animals: Not applicable.

Competing interests: The authors declare no competing interests.

References

1. Pettit, GR. "The dolastatins". *Fortschr Chem Org Naturst*. 70(1997):1-79.
2. Doronina, SO., et al. "Development of potent monoclonal antibody auristatin conjugates for cancer therapy". *Nat Biotechnol*. 21(2003):778-784.
3. Bajjuri, KM., et al. "The legumain protease activated auristatin prodrugs suppress tumor growth and metastasis without toxicity". *ChemMedChem*. 6(2011):54-59.

4. Maderna, A., and Leverett, CA. "Recent advances in the development of new auristatins: Structural modifications and application in antibody drug conjugates". *Mol Pharm*. 12(2015):1798-1812.
5. Singh, SB. "Discovery and development of dolastatin 10-derived antibody drug conjugate anticancer drugs". *J Nat Prod*. 85(2022):666-687.
6. Popova, TV., et al. "Rational design of albumin theranostic conjugates for gold nanoparticles anticancer drugs: Where the seed meets the soil?". *Biomedicines*. 9(2021):74-89.
7. Lisitskiy, VA., et al. "Multifunctional human serum albumin-therapeutic nucleotide conjugate with redox and pH-sensitive drug release mechanism for cancer theranostics". *Bioorg Med Chem Lett*. 27(2017):3925-3930.
8. Elzoghby, AO., et al. "Albumin-based nanoparticles as potential controlled release drug delivery systems". *J Control Release*. 157(2012):168-182.
9. Cho, H., et al. "Emerging albumin-binding anticancer drugs for tumor-targeted drug delivery: Current understandings and clinical translation". *Pharmaceutics*. 14(2022):728-756.
10. Tao, HY., et al. "The development of human serum albumin-based drugs and relevant fusion proteins for cancer therapy". *Int J Biol Macromol*. 187(2021):24-34.
11. Liu, X., et al. "Controlled loading of albumin-drug conjugates *ex vivo* for enhanced drug delivery and antitumor efficacy". *J Control Release*. 328(2020):1-12.
12. Yi, C., et al. "Guanidine-modified albumin-MMAE conjugates with enhanced endocytosis ability". *Drug Deliv.* 30(2023):2219433-2219449.
13. Temming, K., et al. "Evaluation of RGD-targeted albumin carriers for specific delivery of auristatin E to tumor blood vessels". *Bioconjug Chem*. 17(2006):1385-1394.
14. Temming, K., et al. "Improved efficacy αvβ3-targeted albumin conjugates by conjugation of a novel auristatin derivative". *Mol Pharm*. 4(2007):686-694.
15. Renoux, B., et al. "Targeting the tumour microenvironment with an enzyme-responsive drug delivery system for the efficient therapy of breast and pancreatic cancers". *Chem Sci*. 8(2017):3427-3433.
16. Renoux, B., et al. "A β-glucuronidase-responsive albumin-binding prodrug programmed for the double release of monomethyl auristin E". *MedChemComm*. 9(2018):2068-2071.
17. Pes, L., et al. "Novel auristatin E-based albumin-binding prodrugs with superior anticancer efficacy *in vivo* compared to the parent compound". *J Control Release*. 296(2019):81-92.
18. Malouff, TD., et al. "Boron neutron capture therapy: A review of clinical applications". *Front Oncol.* 11(2021):601820-601831.
19. Hughes, AM., and Hu, N. "Optimizing Boron Neutron Capture Therapy (BNCT) to treat cancer: an updated review on the latest developments on boron compounds and strategies". *Cancers*. 15(2023):4091–4121.
20. Kikuchi, S., et al. "Maleimide-functionalized closo-Dodecaborate Albumin Conjugates (MID-AC): Unique ligation at cysteine and lysine residues enables efficient boron delivery to tumor for neutron capture therapy". *J Control Release*. 237(2016):160-167.
21. Nakamura, H., et al. "closo-Dodecaborate-conjugated human serum albumins: Preparation and *in vivo* selective boron delivery to tumor". *Pure Appl Chem.* 90(2018):745–753.
22. Ishii, S., et al. "Design of S-S bond containing Maleimide-conjugated closo-dodecaborate (SSMID): Identification of unique modification sites on albumin and investigation of intracellular uptake". *Org Biomol Chem*. 17(2019):5496-5499.
23. Popova, TV., et al. "Homocystamide conjugates of human serum albumin as a platform to prepare bimodal multidrug delivery systems for boron neutron capture therapy". *Molecules*. 26(2021):6537–6553.
24. Raskolupova, VI., et al. "Design of the new closo-dodecarborate-containing gemcitabine analogue for the albumin-based theranostics composition". *Molecules.* 28(2023):2672-2689.
25. Kashiwagi, H., et al. "Boron neutron capture therapy using dodecaborated albumin conjugates with maleimide is effective in a rat glioma model". *Invest New Drugs*. 40(2022):255-264.
26. Peters, RA. "Mechanism of the toxicity of the active constituent of dichapetalum cymosum and related compounds". *Adv Enzymol Relat Subj Biochem.* 18(1957):113-159.
27. Grin, MA., et al. "New boron-containing bacteriochlorin p cycloimide conjugate". *Russ Chem Bull.* 57(2008):2230-2232.
28. Hawthorne, MF., et al. ".pi.-Dicarbollyl derivatives of the transition metals. Metallocene analogs". *J Am Chem Soc*. 90(1968):879-896.
29. Rak, J., et al. "Solubilization and deaggregation of cobalt bis(dicarbollide) derivatives in water by biocompatible excipients". *Bioorganic Med Chem Lett.* 20(2010):1045-1048.
30. Chubarov, AS., et al. "Design of protein homocystamides with enhanced tumor uptake properties for 19F magnetic resonance imaging". *Bioorg Med Chem.* 23(2015):6943-6954.
31. Mosmann, T. "Rapid colorimetric assay for cellular growth and survival-application to proliferation and cytotoxicity assays". *J Immunol Methods*. 65(1983):55–63.
32. Jeon, SI., et al. "Cathepsin B-responsive prodrugs for cancer-targeted therapy: Recent advances and progress for clinical translation". *Nano Res*. 15(2022):7247-7266.
33. Xu, G., and McLeod, HL. "Strategies for enzyme/prodrug cancer therapy". *Clin Cancer Res*. 7(2001):3314-3324.
34. Era, H., et al. "Heterogeneity of commercially available human serum albumin products: Thiol oxidation and protein carbonylation". *In Proceedings of the 37th Congress of IUPS, Birmingham, UK*. (2013):21-26.
35. Miyamura, S., et al. "Comparison of posttranslational modification and the functional impairment of human serum albumin in commercial preparations". *J Pharm Sci.* 105(2016):1043-1049.
36. Watanabe, H., et al. "Clinical implications associated with the posttranslational modification-induced functional impairment of albumin in oxidative stress-related diseases". *J Pharm Sci.* 106(2017):2195-2203.
37. Oettl, K., and Marsche, G. "Redox state of human serum albumin in terms of cysteine-34 in health and disease". *Methods Enzymol*. 474(2010):181-195.
38. Popova, TV., et al. "Protein modification by thiolactone homocysteine chemistry: A multifunctionalized human serum albumin theranostic". *RSC Med Chem*. 11(2020):1314-1325.
39. Ma, Q., et al. "Cancer stem cells and immunosuppressive microenvironment in glioma". *Front Immunol.* 9(2018):2924-2941.
40. Liu, H., et al. "The role of lysosomal peptidases in glioma immune escape: Underlying mechanisms and therapeutic strategies". *Front Immunol.* 14(2023):154146-154162.
41. Colin, C., et al. "High expression of cathepsin B and plasminogen activator inhibitor type-1 are strong predictors of survival in glioblastomas". *Acta Neuropathol*. 118(2009):745-754.
42. Xie, Z., et al. "Cathepsin B in programmed cell death machinery: Mechanisms of execution and regulatory pathways". *Cell Death Dis*. 14(2023):255-273.
43. Martucci, NM., et al. "Nanoparticle-based strategy for personalized B-cell lymphoma therapy". *Int J Nanomedicine.* 11(2016):6089-6101.
44. Doronina, SO., et al. "Enhanced activity of monomethylauristatin F through monoclonal antibody delivery: Effects of linker technology on efficacy and toxicity". *Bioconjug Chem*. 17(2006):114-124.
45. Maeda, H., et al. "Tumor vascular permeability and the EPR effect in macromolecular therapeutics: A review". *J Control Rel* . 65(2000):271-284.
46. Lin, T., et al. "Blood-brain-barrier-penetrating albumin nanoparticles for biomimetic drug delivery *via* albumin-binding protein pathways for antiglioma therapy". *ACS Nano.* 10(2016):9999-10012.
47. Park, CR., et al. "Secreted protein acidic and rich in cysteine mediates active targeting of human serum albumin in u87mg xenograft mouse models". *Theranostics*. 9(2019):7447-7457.
48. Zhao, P., et al. "Roles of albumin-binding proteins in cancer progression and biomimetic targeted drug delivery". *Chembiochem*. 19(2018):1796-1805.
49. Cui, T., et al. "JNTX-101, a novel albumin-encapsulated gemcitabine prodrug, is efficacious and operates *via* caveolin-1-mediated endocytosis". *Mol Ther Oncolytics.* 30(2023):181-192.

Cite this article: Wang M, et al. Development of Theranostics Albumin Auristatin Conjugates for Combining Chemotherapy with Boron Neutron Capture Therapy. J Biol Todays World, 2024,13(1), 001-007